Hindawi
Journal of Nanomaterials
Volume 2019, Article ID 4508687, 7 pages
https://doi.org/10.1155/2019/4508687

Research Article

Facile Preparation and Enhanced Visible-Light Photocatalysis of ZnO Arrays@BiOI Nanosheets Heterostructures

Da Zhang, Yuanyi Wang, Liang Chen, Chengjing Xiao, Jing Feng, Lingmin Liao, Tao Wei, and Zaiqin Wang

Changjiang River Scientific Research Institute, Wuhan 430010, China

Correspondence should be addressed to Da Zhang; zhangda@mail.crsri.cn

Received 12 May 2019; Accepted 9 October 2019; Published 15 November 2019

Academic Editor: Silvia Licoccia

A simple two-step method of growing ZnO nanorod arrays on the surface of BiOI nanosheets was developed under mild environment. The hierarchical structure of ZnO arrays@BiOI nanosheets was characterized by various measurements like X-ray powder diffraction, scanning electron microscopy, transmission electron microscopy, and energy-dispersive X-ray detector. The optical absorption of the ZnO arrays@BiOI nanosheets composite was investigated by UV-Vis diffuse reflectance spectra. The photocatalytic degradation of methanol orange under visible light shows that the obtained ZnO arrays@BiOI nanosheets heterostructures exhibit enhanced photocatalytic activity, contrasting to the sum of BiOI nanosheets and ZnO nanorods. The mechanism of the photocatalytic process was discussed. This method of growing ZnO nanorod arrays on other nanosheets also provides a potential method to fabricating other complex structures.

1. Introduction

With the development of modern industrial society, environmental pollution and energy shortage have evolved into a global crisis [1, 2]. Photocatalytic technology has been used as a kind of green environmental treatment. However, the use of semiconductor photocatalytic materials such as TiO_2 and ZnO can only be used in the UV light only accounted for less than 5% parts of the solar light [3, 4]. The exploring of visible-light photocatalytic materials is a hotspot among materials and chemical scientists. Recently, much attention has been focused on the plasma catalyst such as Ag/AgCl [5, 6] and Pt/TiO_2 [7–9], which has good visible-light photocatalytic activity. But the containment of noble metal limited its wide application.

Although narrow bandgap semiconductors can absorb visible light, they generate a fast electron-role recombination. The properties of photocatalysts can be adjusted by designing the specific structure, which can effectively improve the charge transfer efficiency [10–12]. Heterogeneous structure formed by two different kinds of semiconductor can effectively promote the separation of electron-role pair and prolong its lifetime [13–17]. The formation of *p-n* heterojunction has been widely used in many fields, such as in the solar energy conversion, because the internal electric field can significantly reduce the carrier recombination, so as to enhance the photocatalytic property [18–21].

In this work, a two-step method is explored to synthesize a ZnO arrays@BiOI nanosheets heterostructures. The heterojunction complex was obtained by the seed growth of ZnO nanorod arrays on the BiOI nanosheets as substrate. Using MO as a model pollutant, the photocatalytic activity of ZnO arrays@BiOI nanosheets was studied under visible light. This method could be applied to synthesis other semiconductor heterostructures with enhanced photocatalytic activity.

2. Experimental Section

2.1. Materials. $Bi(NO_3)_3{\cdot}5H_2O$, KI, ethanol, and MO were of analytical grade and purchased from Shanghai Chemical Reagent Ltd. Deionized water, obtained by means of a water purification system, was used in the experiments.

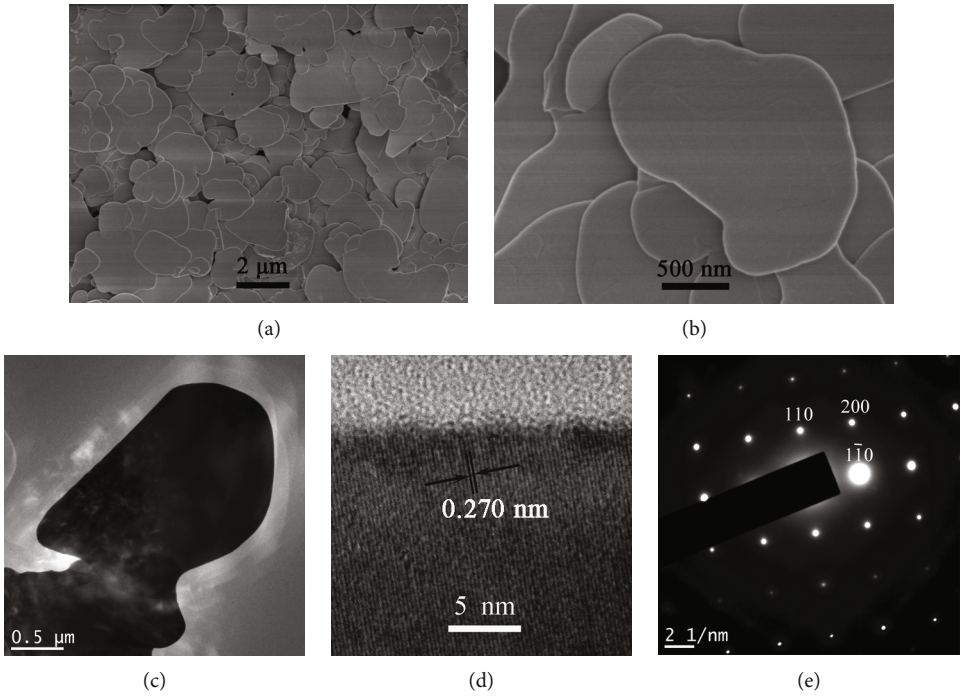

Figure 1: Morphologies of the BiOI nanosheets. (a, b) SEM images, (c) TEM image, (d) HRTEM image, and (e) corresponding selective area electronic diffraction (SEAD) pattern.

2.2. Synthesis of BiOI Crystals. The preparation of BiOI nanosheets was referred to our previous work. 0.1660 g (1 mmol) KI was dissolved in 15 mL deionized water in a three-neck flask and heated to 90°C. Then, 0.4858 g (1 mmol) of $Bi(NO_3)_3{\cdot}5H_2O$ was dispersed into 20 mL absolute ethanol by ultrasonation to get a suspension, which was then added to the above KI solution under 90°C dropwisely. The reaction was maintained at the same temperature for 3 h and then cooled to room temperature naturally. The precipitation was separated by centrifugation and washed with deionized water and absolute ethanol several times, respectively. Finally, the as-obtained product was dried under vacuum at 60°C for further characterization.

2.3. Synthesis of ZnO Sol Solution. 0.2744 g $Zn(CH_3COO)_2{\cdot}2H_2O$ was dissolved in 125 mL ethanol in a beaker and heated to 60°C to get a solution. Then, 65 mL of 0.03 M KOH solution in ethanol was added to the above $Zn(CH_3COO)_2$ solution under 60°C dropwisely. The mixture was maintained at the same temperature for 2 h and obtained the ZnO sol solution.

2.4. Synthesis of ZnO Arrays@BiOI Nanosheets Heterostructures. 20 mg of BiOI nanosheets was dispersed in 100 mL of 0.04 g/L PVP solution and stirred for 3 h. The BiOI nanosheets modified by PVP was separated by centrifugation and washed with absolute ethanol to remove the excess PVP. Then, the modified BiOI nanosheets were dispersed to the above ZnO sol solution, stirred for 3 h, and separated by centrifugation. The precipitation was washed by water and then dispersed to a solution mixed with 10 mL of 0.02 $Zn(NO_3)_2$ and 10 mL of 0.02 M urotropine in a beaker. Then, the beaker was heated to 85°C and maintained for 8 h. The as-obtained product was separated by centrifugation, washed with absolute ethanol several times, and dried under vacuum at 60°C for further characterization.

2.5. Characterization and Photocatalytic Measurement. We followed the methods of Zhang et al., 2016 [22]. XRD patterns of samples were measured on a Bruker D8-advance X-ray diffractometer with Cu Kα radiation ($\lambda = 0.154056$ nm) (Germany), using a voltage of 40 kV, a current of 40 mA, and a scanning rate of 0.02°/s, in 2θ ranges from 10° to 70°. The cell lattice constants of samples were calculated and corrected by MDI Jade (5.0 edition) software. SEM images were acquired on a Hitachi S-4800 scanning electron microscope (SEM). Transmission electron microscopy (TEM, JEM-2100, JEOL) with fast Fourier transformation (FFT) and selected area electron diffraction (SAED) was measured at an accelerating voltage of 200 kV. The thickness of the ultrathin BiOBr was determined by AFM measurement (SPA-300HV, NSK). UV-Vis diffuse reflectance absorbance (DRS) was obtained with a UV-Vis diffuse reflectance spectrometer (BWS003, Newark, DE).

The photocatalytic activity experiments of the different samples for the decomposition of 10 mg/L MO in aqueous solution were performed in a XPA-Photochemical Reactor (Xujiang Electromechanical Plant, Nanjing, China). A 500 W Xeon lamp with a filter ($\lambda \geq 400$ nm) was used to obtain visible light, and the near-infrared light was removed by condensate water around the lamp. A mixture of 40 mL of 10 mg/L MO aqueous solution and 40 mg catalyst were transferred into a quartz tube with a capacity of 50 mL. The above suspension was treated by ultrasonation for 10 min and then magnetically stirred in dark for 1 h to reach adsorption equilibrium of MO with the catalyst. Then, the mixture was

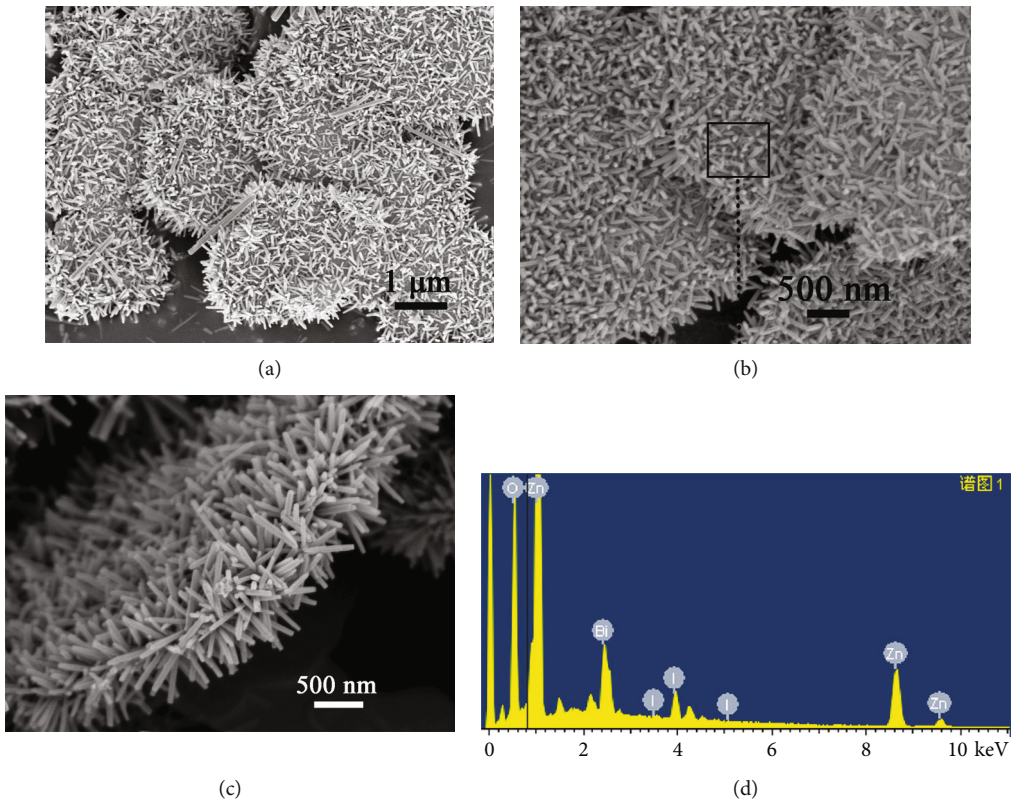

Figure 2: Morphologies of the ZnO arrays@BiOI nanosheets composite (a–c) SEM images and (d) EDX analysis of one single structure.

continuously agitated throughout the experiment and irradiated by the visible light. After a given irradiation time, about 3 mL of the mixture was withdrawn and immediately centrifuged to remove the catalyst. The concentration of RhB was determined by measuring its absorption in the main absorbance with a UV–Vis spectrophotometer (Agilent 8453).

3. Results and Discussion

Figure 1 shows the morphology and structure of the BiOI nanosheets, obtained by a hydrolysis reaction without any agent. The size of the nanosheets is about 3-5 μm, and the thickness is about several hundred nanometers, with irregular circular shape. HRTEM result shows that each BiOI nanosheet is single crystal. The clear lattice fringes can be observed in Figure 1(d), and the crystal plane spacing is about 0.270 nm. The SAED results further verify the structure of single crystals with main {001} facets exposed and the diffraction spots also indicate the typical tetragonal crystal system.

The ZnO arrays@BiOI nanosheets heterostructures were prepared by in situ growing ZnO nanorod arrays on the surface of the as-prepared BiOI nanosheets. Figure 2 shows the morphology and composition of the ZnO arrays@BiOI nanosheets. It can be seen they are relatively uniform in large area from the low-scale SEM. The substrate of the BiOI nanosheets maintained its oriental size of 3-5 μm, while the ZnO nanorods attached to the BiOI surface. From the side direction, we can see that a large number of ZnO nanorods grew densely on both sides of the BiOI nanosheets in Figure 2(c). The EDX energy spectrum analysis was carried out on the surface of the composite. The signal results contain the total elements of ZnO and BiOI, and the signal intensity of Zn is much higher than that of Bi, because the ZnO is covering on the surface of BiOI.

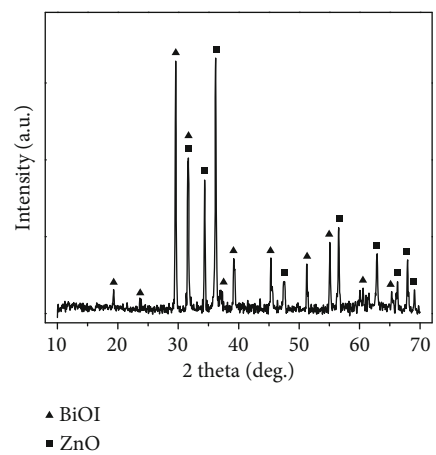

Figure 3: XRD patterns of the ZnO arrays@BiOI nanosheets composite.

The composition of the material was characterized by the XRD method. The XRD pattern of the as-prepared ZnO arrays@BiOI nanosheets composite shows well-resolved diffraction peaks in Figure 3, of which the peaks labeled "▲" match well with tetragonal BiOI (JCPDS 10-0445), while the peaks labeled "■" peaks are in agreement with those of hexagonal wurtzite ZnO (JCPDS 36-1451).

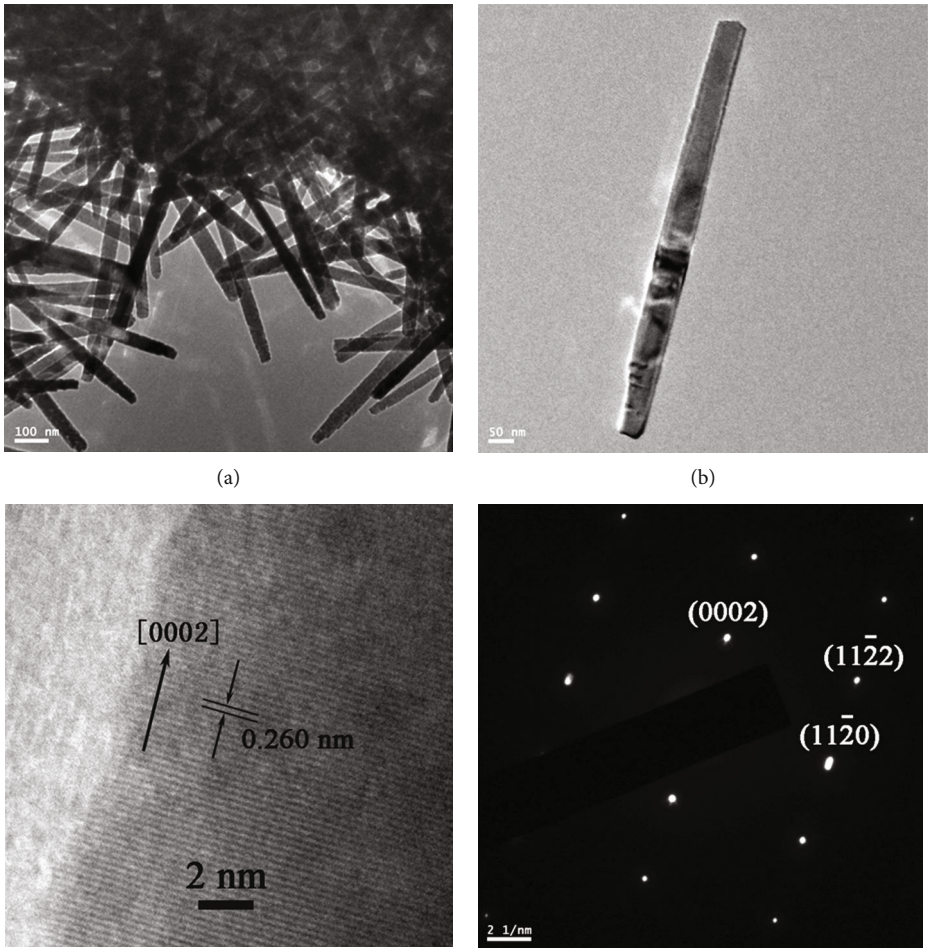

Figure 4: (a, b) TEM images of the composite and the ZnO nanorods, (c) HRTEM image of a single ZnO nanorod, and (d) corresponding selective area electronic diffraction (SEAD) pattern.

There was no characteristic peak for impurities, showing that the product is composed of phase pure ZnO and BiOI. The diffraction peak is sharp, and the crystallinity of the product is good.

Further, the growth process of the ZnO nanorod arrays was confirmed by HRTEM and SAED. The results in Figure 4 show that the ZnO nanorods exfoliated from the surface of BiOI substrate. The diameter of ZnO nanorods is about 50 nm, and the size of ZnO nanorods seems to be very uniform. The TEM and HRTEM images for a single particle are showed in Figures 4(b) and 4(c), and we also got the corresponding SAED spot patterns, showing that the crystal structure with clear lattice fringes of each single crystal is good, and which is characterized by [0002] orientation.

The UV-Vis diffuse reflectance spectra of different samples are shown in Figure 5. The ZnO nanorods have an absorption located at about 370 nm, while BiOI has broader absorption in the visible region with an absorption edge of around 680 nm. The sample of ZnO arrays@BiOI nanosheets composite shows light brown powder, and there were two obvious absorption peaks in the region of nm 200-700, mainly containing the absorption of ZnO nanorods and BiOI

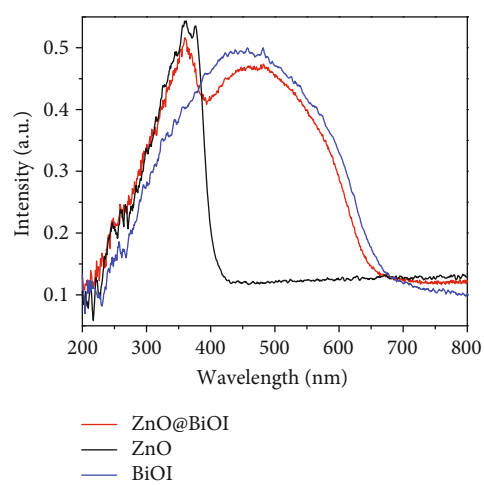

Figure 5: UV-Vis diffuse reflectance spectra of the different samples.

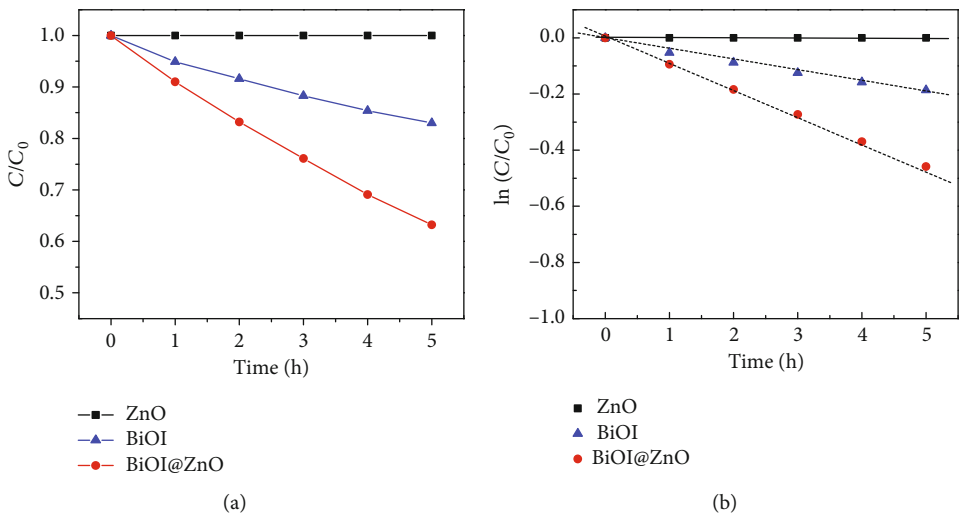

Figure 6: (a) The photodegradation efficiencies of different catalysts under visible light and (b) the calculated rate constants.

nanosheets. Corresponding to the absorption of BiOI, the absorption band edge of ZnO arrays@BiOI nanosheets composite has an obvious blue shift. The reason may be attributed to the interaction of the two kinds of semiconductors.

The photocatalytic activity of the heterogeneous ZnO arrays@BiOI nanosheets composite was measured by decomposing of methyl orange (MO) under visible light, which is a kind of organic dye with stable structure. Figure 6 shows the degradation process of different catalysts including ZnO nanorods, BiOI nanosheets, and ZnO arrays@BiOI nanosheets composite as a function of irradiation time. The results show that the MO concentration does not change in the presence of ZnO nanorods, because ZnO cannot be excited by visible light. After 5 h of irradiation, about 17% of MO molecule was decomposed by BiOI nanosheets. As for ZnO arrays@BiOI nanosheets composite, 37% of MO molecule was decomposed and the photocatalytic activity was significantly enhanced. The degradation process was basically in accordance with the quasi one kinetic equation as following. In the equation, C, C_0, and k indicated the initial concentration of MO solution, the real-time concentration of MO solution, and the reaction rate constant, respectively. The degradation rate k of BiOI was 0.0382 h^{-1}, while the k value of ZnO arrays@BiOI nanosheets composite was 0.0965 h^{-1}, which is 2.52 times than that of pure BiOI nanosheets. Also, the phase and morphologies of ZnO arrays@BiOI nanosheets composite after photocatalytic experiment remain unchanged.

$$\mathrm{Ln}(C/C_0) = -kt. \quad (1)$$

As is well known, the separation and lifetime of photon-generated carrier greatly affected the photocatalytic efficiency in photodegradation process. When two kinds of semiconductors with matched bandgap formed a heterojunction, the photogenerated electrons can flow from the conduction band of one semiconductor to the lower conduction band of another. Based on the experimental and theoretical results, the scheme of band levels about the ZnO nanorods@BiOI

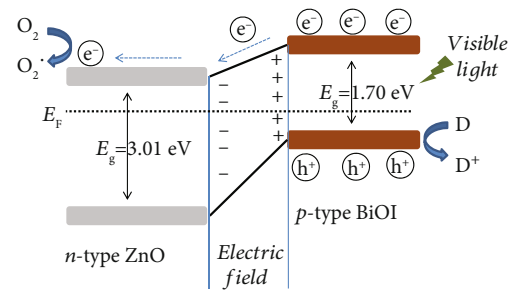

Figure 7: The formation of p-n junction and the proposed charge separation process in ZnO arrays@BiOI nanosheets heterostructures under visible light.

nanosheets composite is shown in Figure 7. The bandgaps of as-obtained ZnO nanorods and BiOI nanosheets were about 1.70 eV and 3.01 eV, respectively. BiOI is a p-type semiconductor, and the Fermi level is close to the valence band. ZnO is an n-type semiconductor with its Fermi level close to the conduction band. When p-n junction formed by combining ZnO nanorods and BiOI nanosheets, the light-produced electrons can diffuse from the conduction band of BiOI to the conduction band of ZnO, resulting in the accumulation of negative charge at the BiOI side of the junction. Accordingly, positive charge accumulated at the ZnO interface of the junction. When the BiOI and ZnO reached equilibrium at the Fermi level, an inner electric field will generate at the interface preventing the charge transfer between the two materials. Under the visible light irradiation, the holes and electrons generated in BiOI will transfer by the above descripted process, which improved the separation efficiency of holes and electrons. Furthermore, the ZnO nanorod arrays provide more active site and obviously help the photocatalytic reaction.

4. Conclusions

In summary, ZnO arrays@BiOI nanosheets composites with p-n heterojunction were obtained by *in situ* growing ZnO

nanorod arrays on the surface of BiOI nanosheets. The structure, morphology, and optical properties of ZnO arrays@-BiOI nanosheets were carefully investigated. Using MO as simulated contaminant, the visible-light catalytic activity of ZnO nanorods, BiOI nanosheets, and BiOI/ZnO composite was studied. The result shows that the ZnO arrays@BiOI nanosheets heterojunction material has much higher catalytic efficiency than the sum of the other two, due to the formation of *p-n* heterojunction. It promoted the separation of photogenerated carriers in the composite interface, thus significantly enhanced the photocatalytic performance.

Data Availability

The data used to support the findings of this study are available from the corresponding author upon request.

Conflicts of Interest

The authors declare that there is no conflict of interests regarding the publication of this paper.

Acknowledgments

The authors are grateful to the financial support of the National Natural Science Foundation of China (Nos. 51609021, 51579019). Thanks are due to the support by Innovation Team and the fundamental research funds (CKSF2017056/CL, CKSF2017039/CL, CKSF2017020/CL) of the Changjiang River Scientific Research Institute.

Supplementary Materials

Figure S1: SEM images of the ZnO/BiOI composite product after photocatalytic experiment. Figure S2: the BET result of the ZnO/BiOI composite product. Figure S3: the spectra of pure ZnO arrays and ZnO/BiOI composite product. *(Supplementary Materials)*

References

[1] M. R. Hoffmann, S. T. Martin, W. Choi, and D. W. Bahnemann, "Environmental applications of semiconductor photocatalysis," *Chemical Reviews*, vol. 95, no. 1, pp. 69–96, 1995.

[2] H. Tong, S. Ouyang, Y. Bi, N. Umezawa, M. Oshikiri, and J. Ye, "Nano-photocatalytic materials: possibilities and challenges," *Advanced Materials*, vol. 24, no. 2, pp. 229–251, 2012.

[3] H. G. Yang, C. H. Sun, S. Z. Qiao et al., "Anatase TiO_2 single crystals with a large percentage of reactive facets," *Nature*, vol. 453, no. 7195, pp. 638–641, 2008.

[4] Y. H. Si, Y. Xia, S. K. Shang et al., "Enhanced visible light driven photocatalytic behavior of $BiFeO_3$/reduced graphene oxide composites," *Nanomaterials*, vol. 8, no. 7, p. 526, 2018.

[5] P. Wang, B. Huang, X. Qin et al., "Ag@AgCl: a highly efficient and stable photocatalyst active under visible light," *Angewandte Chemie International Edition*, vol. 47, no. 41, pp. 7931–7933, 2008.

[6] J. Yu, G. Dai, and B. Huang, "Fabrication and characterization of visible-light-driven plasmonic photocatalyst Ag/AgCl/TiO_2 nanotube arrays," *Journal of Physical Chemistry C*, vol. 113, no. 37, pp. 16394–16401, 2009.

[7] Y. Tian and T. Tatsuma, "Mechanisms and applications of plasmon-induced charge separation at TiO_2 films loaded with gold nanoparticles," *Journal of the American Chemical Society*, vol. 127, no. 20, pp. 7632–7637, 2005.

[8] J. Yu, L. Qi, and M. Jaroniec, "Hydrogen production by photocatalytic water splitting over Pt/TiO_2 nanosheets with exposed (001) facets," *Journal of Physical Chemistry C*, vol. 114, no. 30, pp. 13118–13125, 2010.

[9] Y. Huang, D. Chen, X. Hu, Y. Qian, and D. Li, "Preparation of TiO_2/carbon nanotubes/reduced graphene oxide composites with enhanced photocatalytic activity for the degradation of rhodamine B," *Nanomaterials*, vol. 8, no. 6, p. 431, 2018.

[10] Z. Y. Jiang, Q. Kuang, Z. X. Xie, and L. S. Zheng, "Syntheses and properties of micro/nanostructured crystallites with high-energy surfaces," *Advanced Functional Materials*, vol. 20, no. 21, pp. 3634–3645, 2010.

[11] S. Sun, W. Wang, and L. Zhang, "Bi_2WO_6 quantum dots decorated reduced graphene oxide: improved charge separation and enhanced photoconversion efficiency," *Journal of Physical Chemistry C*, vol. 117, no. 18, pp. 9113–9120, 2013.

[12] X. Zhang, Z. Ai, F. Jia, and L. Zhang, "Generalized one-pot synthesis, characterization, and photocatalytic activity of hierarchical BiOX (X = Cl, Br, I) nanoplate microspheres," *Journal of Physical Chemistry C*, vol. 112, no. 3, pp. 747–753, 2008.

[13] D. Zhang, J. Li, Q. Wang, and Q. Wu, "High {001} facets dominated BiOBr lamellas: facile hydrolysis preparation and selective visible-light photocatalytic activity," *Journal of Materials Chemistry A*, vol. 1, no. 30, pp. 8622–8629, 2013.

[14] X. Liu, Z. Fang, X. Zhang, W. Zhang, X. Wei, and B. Geng, "Preparation and characterization of Fe_3O_4/CdS nanocomposites and their use as recyclable photocatalysts," *Crystal Growth & Design*, vol. 9, no. 1, pp. 197–202, 2009.

[15] Z. Wang, B. Huang, Y. Dai et al., "Highly photocatalytic ZnO/In_2O_3 heteronanostructures synthesized by a coprecipitation method," *Journal of Physical Chemistry C*, vol. 113, no. 11, pp. 4612–4617, 2009.

[16] M. Shang, W. Wang, L. Zhang, S. Sun, L. Wang, and L. Zhou, "3D Bi_2WO_6/TiO_2 hierarchical heterostructure: controllable synthesis and enhanced visible photocatalytic degradation performances," *Journal of Physical Chemistry C*, vol. 113, no. 33, pp. 14727–14731, 2009.

[17] H. Huang, D. Li, Q. Lin et al., "Efficient degradation of benzene over $LaVO_4$/TiO_2 nanocrystalline heterojunction photocatalyst under visible light irradiation," *Environmental Science & Technology*, vol. 43, no. 11, pp. 4164–4168, 2009.

[18] S. Y. Chai, Y. J. Kim, M. H. Jung, A. K. Chakraborty, D. Jung, and W. I. Lee, "Heterojunctioned BiOCl/Bi_2O_3, a new visible light photocatalyst," *Journal of Catalysis*, vol. 262, no. 1, pp. 144–149, 2009.

[19] J. Jiang, X. Zhang, P. Sun, and L. Zhang, "ZnO/BiOI heterostructures: photoinduced charge-transfer property and enhanced visible-light photocatalytic activity," *Journal of Physical Chemistry C*, vol. 115, no. 42, pp. 20555–20564, 2011.

[20] M. Wen, J. Wang, R. Tong et al., "A low-cost metal-free photocatalyst based on black phosphorus," *Advanced Science*, vol. 6, no. 1, article 1801321, 2019.

[21] X. Hu, P. Xu, H. Gong, and G. Yin, "Synthesis and characterization of WO_3/graphene nanocomposites for enhanced photocatalytic activities by one-step in-situ hydrothermal reaction," *Materials*, vol. 11, no. 1, p. 147, 2018.

[22] D. Zhang, L. Chen, C. Xiao et al., "Facile synthesis of high {001} facets dominated BiOCl nanosheets and their selective dye-sensitized photocatalytic activity induced by visible light," *Journal of Nanomaterials*, vol. 2016, Article ID 5697672, 7 pages, 2016.